Pferdeheilkunde – Equine Medicine 39 (2023) 6 (November/December) 504–514 DOI 10.21836/PEM20230601

3D printed and punched porous surfaces of a non-resorbable, biphasic implant for the repair of osteochondral lesions improves repair tissue adherence and ingrowth

Maria C. Fugazzola[1], Nasim Golafshan[2,3*], Joris A. van Aken[2], Saskia Plomp[1], Janny De Grauw[1], Ward van Buul[4], Gied Hermsen[4], Harrie Weinans[2,5], Miguel Castilho[2,3,6], René van Weeren[1] and Jos Malda[1,2,3]*

[1] Department of Clinical Sciences, Faculty of Veterinary Science, Utrecht University, The Netherlands
[2] Department of Orthopedics, University Medical Center Utrecht, Utrecht, The Netherlands
[3] Regenerative Medicine Center, Utrecht, The Netherlands
[4] Joinstphere Company Vestdijk 134, 5611 CZ Eindhoven, The Netherlands
[5] Department of Biomechanical Engineering, TU Delft, Delft, 2628 CD, The Netherlands
[6] Department of Biomedical Engineering, Eindhoven University of Technology, Eindhoven, The Netherlands

Summary: The objective of this study was to evaluate a non-resorbable implant for the focal repair of osteochondral defects. Enhanced adherence of repair cartilage overgrowing the implants was the secondary goal and was tested by introducing porosities on the articular surface of the implant. This study evaluated four versions of the construct composed of a polycarbonate-urethane-urea biomaterial (elastomer) and a bone anchor. In order to induce porosities on the surface of the implant, either vertical holes were punched into it, or the chondral component was 3D-printed onto the implant. Fabrication, biomechanical characterization and cell infiltration of the implant were evaluated *in-vitro*. Subsequently the implants were tested in an *in-vivo* study in four Shetland ponies for 5 weeks. Enhanced porosity was successfully obtained for all implants. The 3D-printing of the elastomeric material produced pore diameters of 775μm and 690μm whilst the micro-punched pores had a diameter of 319μm. The elastic modulus of the elastomer decreased with the introduction of porosity but stayed above values of native cartilage in all versions of the implant. Clinically the implant was well tolerated. The over-growing repair tissue was mostly flush with surrounding cartilage and attached to the elastomer through ingrowth of the tissue into the pores. Overall the tested implants all showed good mechanical performance *in vitro* and subjectively also *in vivo*. The repair cartilage was solidly attached to the porous surface of the implant. The printing approach potentially enables fine-tuning of the biomechanical properties of the implant depending on the specific requirements for a given location.

Keywords: cartilage, Joint, 3D printing, osteoarthritis, implant, horse model

Citation: Fugazzola M. C., Golafshan N., van Aken J. A., Plomp S., De Grauw J., van Buul W., Hermsen G., Weinans H., Castilho M., van Weeren R., Malda J. (2023) 3D printed and punched porous surfaces of a non-resorbable, biphasic implant for the repair of osteochondral lesions improves repair tissue adherence and ingrowth. Pferdeheilkunde 39, 504–514; DOI 10.21836/PEM20230601

Correspondence: Maria Carlotta Fugazzola, Department Equine Sciences, Utrecht University, Yalelaan 112, 3584CM Utrecht, The Netherlands, m.c.fugazzola@uu.nl

Submitted: June 23, 2023 | **Accepted:** September 3, 2023

Introduction

The need for optimal functional treatment of chondral and osteochondral defects in human and veterinary patients is still unmet. Cartilage lesions, if left untreated, ultimately lead to a degenerative catabolic cascade within the joint that eventually develops into osteoarthritis (*Hunziker* 1999, *Mankin* 1982). In a functional therapeutical approach, non-resorbable implants consisting of polymers, alone or combined with metals, have been applied clinically in large-animal models, as well as in humans (*Martinez Carranza* et al. 2019, 2016, *Husby* et al. 2016, *Nathwani* et al. 2017, *Danielski* and *Farrell* 2018, *Becher* et al. 2011). The disadvantage of these types of implants, remains their continuous wear due to exposure at the joint surface and differing biomechanical characteristics between implants and surrounding native cartilage. Further, their success also depends on the condition of the opposing cartilage surfaces (*Damen* et al. 2020).

A novel type of bi-layered, non-resorbable osteochondral implant has been tested recently in a horse model (*Korthagen* et al. 2019). Different to other prosthetic implants, this one is placed just below the articular surface allowing repair tissue to grow over it, creating a flush transition between the neo-tissue, which grows over the implant, and the adjacent original cartilage. The rationale behind this approach is that in these circumstances also a thin layer of fibrocartilage may lead to durable functional repair, which is, unlike surfaces made of artificial materials, self-maintaining. In that pilot study, the implant was completely covered with smooth repair tissue after 12 weeks and the neo-tissue exhibited good adherence to the surrounding native cartilage. However, the repair tissue did

not attach to the underlying elastomer, making it easily glide over the elastomer's surface (*Korthagen* et al. 2019).

In the present study, we aimed to improve the mechanical stability of the repair tissue on the elastomer. To achieve improved attachment of the over-growing repair tissue, we first roughened the upper surface of the elastomeric implant by punching vertical pores into its surface to facilitate tissue ingrowth. When this approach appeared to have the desired effect, we increased the implants' porosity in a more controlled manner, using a 3D printing-based fabrication process for the elastomer. We hypothesized that the 3D character architecture of the pores would induce not only vertical, but also horizontal fibrocartilage ingrowth, further fomenting tissue integration. In order to assess the mechanical performance after the introduction of porosity, the mechanical and biological proprieties of the implants were initially evaluated *in vitro*. Subsequently, the implants were tested in a pilot equine experimental model.

Material and Methods

The tested implants all were composed by a chondral component consisting of polycarbonate-urethane-urea biomaterial (PCUU elastomer) and a bone anchor consisting of polyetherketoneketone (PEKK). Four versions of the implant were manufactured and differed from each other only in the chondral component of its bi-layered structure. The previously tested version of the implant (*Korthagen* et al. 2019), with a smooth surface (smooth elastomer: SE) was compared in a study in two ponies to a new version in which the chondral component contained vertical micro-punched pores (punched elastomer: PE). The other two manufactured implants contained 3D-printed versions of the elastomeric urethane on top of the bone anchor component. They differed from each other only by the size of the printed pores (3D-printed large pores, 3D-L and 3D-printed small pores, 3D-S). These two versions were compared in a second pilot in two further ponies. Only the three new versions PE, 3D-L and 3D-S were tested mechanically and *in-vitro*, whilst all four versions (including SE) were tested *in-vivo*.

Preparation of chondral component of the implant

Punched elastomer (PE) and smooth elastomer (SE)

The SE implant was fabricated using a Polycarbonate-urethane-urea biomaterial (PCUU elastomer; PolyVation B.V., Groningen, the Netherlands) and was left untreated, as previously described (*Korthagen* et al. 2019). For the PE, 14 equally distributed pores with a diameter of 319 μm and a depth of 800 μm were punched into the elastomer with a custom-made owl. The optimum pore-size for cell-infiltration and practical manufacturing had been determined previously (Fig. S1).

3D-printing for 3D-L and 3D-S

The biomaterial ink was prepared by dissolving 180 mg/ml PCUU in 5 v/v% trifluoroacetic acid (TFA) in dichloromethane (DCM) (Sigma-Aldrich, Germany) for 24 hours. PCUU implants with smaller (3D-S) and larger (3D-L) pores were printed using an extrusion-based 3D-printing system (3DDiscovery, regenHu, Switzerland). The ink was transferred to a 3 mL syringe (Nordson EFD, USA) and extruded through a 27G conical nozzle, 0.2 mm (Nordson EFD, USA). Continuous ink deposition was achieved by applying a pneumatic pressure of 1.3 bar at 2 mm/s. Printability of the biomaterial ink was first evaluated by a filament fusion test according to a protocol described elsewhere (*Golafshan* et al. 2021) (Suppl. 1).

Structural characterization of the printed product

The surface morphology of the chondral component was evaluated using a stereomicroscope (Olympus SZ61) and the pore size of the 3D printed implants was analyzed using a Scanning Electron Microscope (XL30SFEG, FEI, USA) at an acceleration voltage of 10 kV. The porosity of the chondral components was evaluated by Image J (public source program) comparing area of pores and elastomer material.

Assessment of mechanical properties of PE, 3D-L and 3D-S

Implants were characterized under uniaxial compression using a universal testing machine (Zwick Z010, Germany) equipped with a 1 kN load cell (0.2 mm/min). Dynamic compression tests were performed by applying a ramp force to a height of 2 mm (equivalent to a strain of 20 %) followed by a sinus wave deformation at a frequency of 0.1 Hz. The methods used to obtain all resulting mechanical parameters are described in the supplementary section (Suppl. 2).

In vitro cell culture of PE, 3D-L and 3D-S

Three groups containing each 3 sterilized samples of PE, 3D-L and 3D-S were seeded with equine cartilage progenitor cells at a density of 30,000 cells per sample (d = 5 mm, h = 1 mm) and cultured for 14 days as described (Suppl. A). Samples were taken at day 1 and day 14 after seeding (3 samples per group). At both timepoints, cell metabolic activity was quantified using the Alamar blue assay (ThermoFischer), following manufacturer's instruction, while DNA content was measured using a Qubit dsDNA BR assay (ThermoFisher) according to the manufacturer's protocol. Imaging techniques are described in the supplementary material and methods (Suppl. 3).

Fabrication of the osteochondral implants

The bone component of the osteochondral implant was made of polyetherketoneketone (PEKK) that anchors the implant to the native subchondral bone. In order to fixate the PE on the PEKK bone anchor, a layer of 0.2 mm PCUU was compression-moulded onto the PEKK after which the PE was ´glued' on top of that using a 5 %TFA/DCM solution. The SE was manufactured identically.

For the 3D-L and 3D-S, the PEKK was placed in a negative mould and PCUU was printed on top of the mould. The fabrication process is schematically shown in Fig. S3.

In-vivo evaluation

Experimental set up

In a first experiment the SE was compared to the PE in two ponies (each stifle receiving a different implant). The diameter of these plugs was 6 mm and total height was 7 mm. In the second experiment the two 3D printed versions were compared in two ponies. The diameter of these plugs was increased to that of a critical-size defect of 10 mm and total height was 7 mm. The animals were female adults, with mean age 5 years (range 4 to 9), weighing between 200 and 270 kg. Further inclusion criteria are described in Supplementary material and methods.

The experiments were carried out with the approval of the Animal Welfare Body Utrecht (IvD Utrecht, Project number AVD1080020186885).

Surgical procedure

First experiment – SE vs PE
Pre-operative preparation and anesthesia followed routine protocols (see Supplementary material and methods). After surgical preparation, bilaterally a medial femoro-patellar and a femoro-tibial arthrotomy were performed and 4 implants per pony were placed, 2 in each stifle. For both ponies a SEs implant of 6 mm in diameter was placed in the medial trochlea and another one in the medial condyle of the right stifle. Similarly, PEs implants of the same diameter and in the same two locations were placed in the left stifle, again for both ponies. The defects were made on the axial side of the medial trochlea, halfway between the apex of the patella and the most proximal aspect of the tibial tuberosity and on the weightbearing surface of the medial femoral condyle. The osteochondral defects (6 mm diameter and 7.5 mm depth) were created using a customized drill bit and drill sleeve. The rim of the round defect was trimmed until a clean perpendicular cartilage border was obtained. The implant was inserted manually and carefully press-fitted with a custom-made punch until the elastomer was about 0.5 mm below the surrounding cartilage surface. The depth of placement was assessed subjectively. After flushing the surgical site with saline, the joint was closed in 4 layers and a stent was placed over the incision.

Second experiment – 3DP-L vs 3DP-S
To test the two 3D-printed implant versions (both 10 mm in diameter), a similar procedure was performed in two additional animals. In total 2 implants where used per pony. A 3DP-L was placed in the right stifle in the medial trochlear ridge and the 3DP-S in the left stifle at the same site.

Post-mortem evaluation
After 5 weeks, general anesthesia was induced with midazolam (0.06 mg/kg) and ketamine (2.2 mg/kg) and the ponies were humanely euthanized with an overdose of Pentobarbital. The joints were exposed and macroscopic assessment performed by visual inspection and palpation. Any signs of kissing lesions or macroscopic changes in the joint were recorded. It was attempted to displace the overgrowing tissue by hand with an arthroscopic probe. When the tissue appeared firmly attached to the elastomer, a rectangular osteochondral block of cartilage and bone containing the plug was harvested. The blocks were fixated in formalin and later embedded in Polymethylmetacrylate (PMMA). After hardening, the PMMA embedded plug was cut with a Leica 4 SP1600 Saw Microtome system (Leica) to yield 50–60 μm sections and stained with basic fuchsine-methylene blue. The sections were analyzed for signs of tissue ingrowth into the pores or into the 3D-printed structure of the elastomer, respectively. A sagittal section of one of the pores of each implant was used to measure the surface of the tissue core in the pore as a quantitative approximation of tissue ingrowth. This ingrowing tissue area was measured three times with a digital image analysis tool (Image J) and averaged.

Statistical analysis

Statistical analyses of mechanical proprieties and in vitro culture were performed using GraphPad prism V6. Data were represented as mean ± standard deviation. The significance of differences between the three groups was assessed using a one-way ANOVA and post-hoc Tukey's test. Differences were considered significant at a probability error (p) of $p < 0.05$.

Results

Implant fabrication

The osteochondral implants with enhanced porosity were successfully generated using two techniques: by the introduction of punched pores and by 3D-printing of the elastomeric material (Fig. 1). Prior to 3D-printing of the implants, the filament fusion investigation of the elastomeric biomaterial ink revealed that the minimum inter-fiber spacing for a single layer that could be achieved was 800–1000 μm (Fig. S2). Based on this, two pore sizes (0.8 mm and 1 mm) were selected for chondral implant fabrication. The experimental average pore diameter achievable for multiple layers of 3D-S and for 3D-L versions was 690 μm and 775 μm, respectively. The overall average porosity of the cartilage phase of the PE implants was 2.1 %, while for the 3D-S and 3D-L this was 40.2 % and 67.4 %, respectively (Fig. 1B). Underscoring the significant differences in the surface morphology of the three different implants (Fig. 1C-E).

Mechanical properties

The stress-strain curve of the various implants under quasi static compression is shown in Fig. 2A. The increase of porosity resulted in a decrease in both elastic modulus and yield stress of the elastomers. The elastic modulus of PE, 3D-S, and 3D-L are 24.9 MPa, 16.1 MPa, and 3.8 MPa, respectively

(Fig. 2C). Moreover, the yield stress of PE, 3D-S, and 3D-L are 23.3 MPa, 8.4 MPa, and 4.2 MPa, respectively (Fig. 2D). The strain energy for PE was 6 times higher than for the 3D-L (Fig. 2E). Further, recovery and energy dissipated under cyclic loading at 20% strain was evaluated for 20 cycles. Interestingly, all three elastomer versions could resist over 20 cycles of compression without sign of any permanent deformation (Fig. 2F). Moreover, the recovery percentage of the elastomer was the highest for the elastomer with the higher porosity (Fig. 2G). The energy dissipation was inversely proportioned to the porosity of the implant, being highest for the punched pore elastomer (PE).

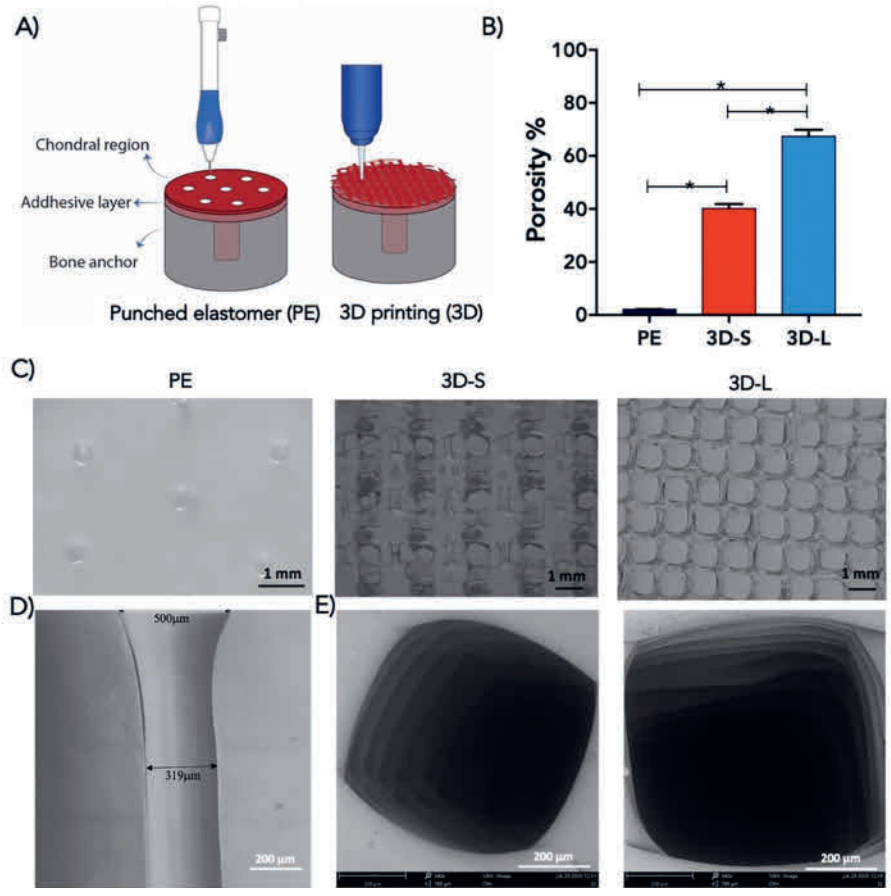

Fig. 1 A) Illustration of the fabrication procedure of the implants. B) The porosity of the chondral component for all the versions of the implants. C) Stereomicroscopic images of the implants. D) Microscopic transverse section of PE. E) SEM cross-sectional images of the pores of the implants 3D-S and 3D-L.

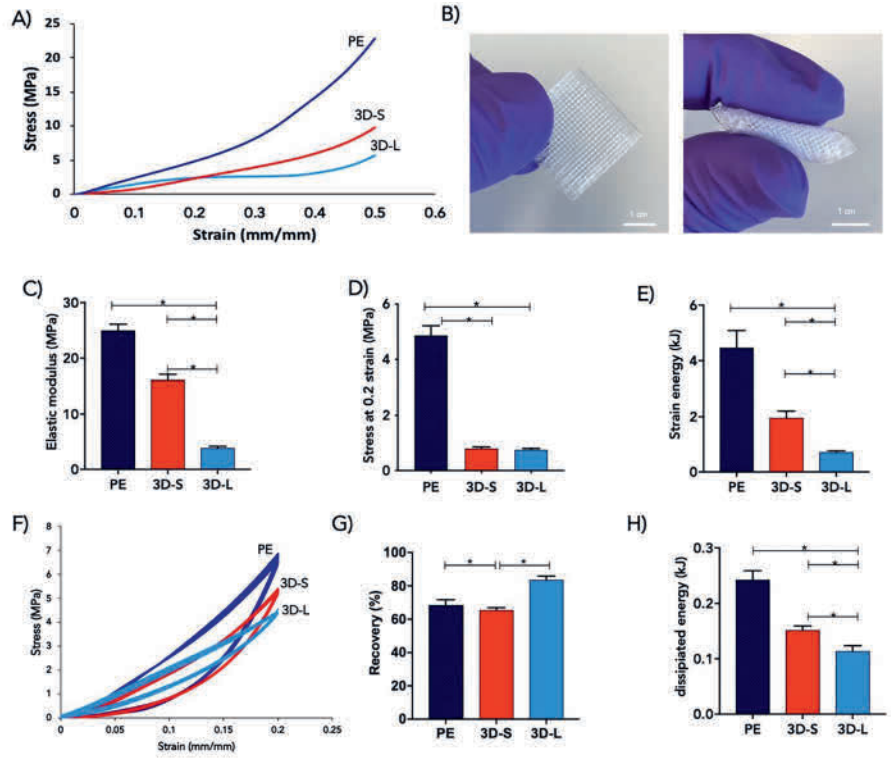

Fig. 2 A) Longitudinal compression profile of implants. B) Photographic illustration of the elastic behavior of the implants. C) Elastic modulus, D) Stress at 0.2 mm/mm strain, and E) strain energy from compressive loading profile for various implants. F) The cyclic compression profile for various implants (20 cycles). G) recovery and H) Dissipated energy of the implants after each test.

Cytocompatibility and cell infiltration of porous chondral parts

To evaluate the cytocompatibility and the cell infiltration capability of the implants, articular cartilage progenitor cells were cultured on the implants for 14 days. The metabolic activity analysis confirmed that the cells were active during the whole duration of the *in vitro* study (Fig. 3A). Moreover, no negative effects on cell activity were observed as a result of the use of a solvent-based extrusion printing approach. The quantitative DNA measurements revealed an increase of DNA over time for all the implants from day 1 to day 14. (Fig 3B). Cell nuclei staining evaluated the infiltration of the cells into the pores of the implant and were visible after 14 days of culture (Fig 3C).

Surgery and clinical outcome

In the first *in vivo* pilot, comparing SE and PE, all 8 implants (4 per pony) were placed successfully in the two desired locations (medial condyle and medial trochlea). In the subsequent *in vivo* pilot, comparing 3D-L and 3D-S, 4 plugs of 10 mm diameter were to be placed in the medial trochlea. However, two out of four implants could not be completely placed below the articular surface. In these cases, one third of the implant surface was flush with the articular surface, but not below the surface, as desired. Post-operative recovery was good in all ponies. After removing the surgical stents on the third day post-operatively, the animals showed unhindered motion. Surgical wounds healed uneventfully, and a mild effusion of all treated stifle joints remained throughout the study. At 5 weeks the animals did not show any signs of lameness. Oblique radiographs depicting the medial trochlea showed the implant in place with no to mild sclerosis and no signs of lysis in the surrounding bone for all three types of implants (Fig. 4C).

Macroscopic outcome and subjective mechanical testing

At necropsy, 5 weeks after surgery, the implant location was clearly visible. In the SE vs PE experiment, the implants on the medial trochlea were covered with newly-formed tissue, which differed in color and thickness between the two animals (Fig. 4D). When being pushed with a metallic probe, the tissue covering the SE, slid off the surface with no resistance, once it was not anymore attached to adjacent cartilage. In the other implant with punched pores, the tissue could not be moved over the surface and the whole implant unit could be conserved intact for histological evaluation. In the femoral condyles, only partial covering of the implant from the borders was visible. This tissue appeared thicker and glossier that the tissue covering the medial trochlea (Fig. 5). The difference in resistance of repair tissue to manual displacement with the probe between the two types of implant was the same as for the trochlea implantation sites.

In the second experiment comparing the two 3D printed implants, two out of four implants on the medial trochlear showed overgrowth of tissue (Fig. 4D). The two implants that could not be placed correctly during surgery were covered only by 50 % in one case and not covered at all in the other case. The portion of the implant that had been flush with and not below the surface, was slightly protruding at the post-mortem examination. The newly overgrown tissue of all implants resisted mechanical probing and could not be dislocated or detached from the elastomer. There was no macroscopic difference between the two 3D-printed versions of the elastomer with different pore sizes.

Histologic outcome

Histology revealed that the implants from the SE vs PE experiment showed ingrowth of tissue into the punched (PE) pores (Fig. 6). Cells could be seen within the ingrowing tissue. Depth of ingrowth was 100 µm. The transition to the surrounding cartilage was confluent, without step formation or interruption, even though a clear demarcation between native and repair tissue could be observed. Trabecular bone was surrounding the PEKK implant and new bone formation around the PEKK was seen in some sections. In the experiment comparing the two 3D-printed versions, tissue ingrowth occurred in both 3D-L and 3D-S. Depth of ingrowth was 100 µm in both versions (Fig. 6). No tissue was seen in deeper layers and no horizontal ingrowth was visible. Also here, the bone was tightly surrounding the PEKK and newly formed bone could be detected adjacent to the PEKK.

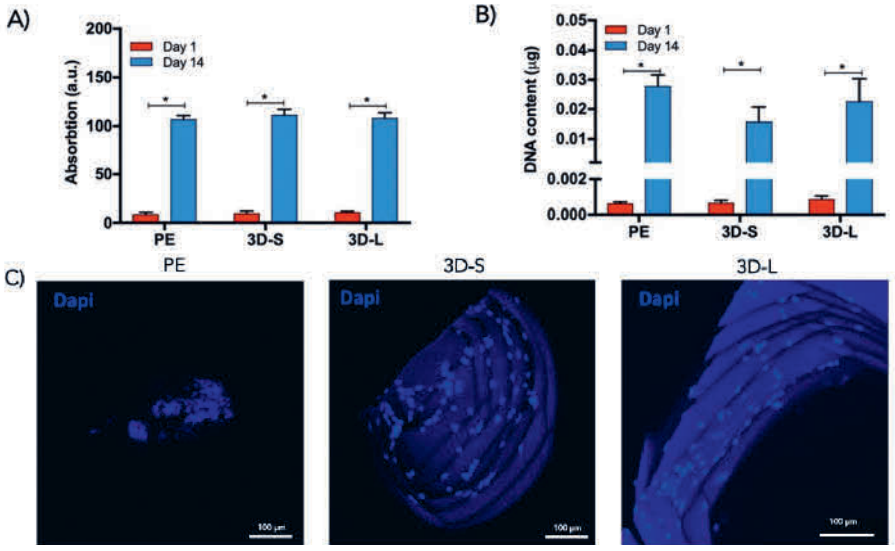

Fig. 3 A) Metabolic activity and B) DNA content of Articular Cartilage Progenitor Cells (ACPCs) during 14 days of culturing. C) DAPI staining of infiltrated ACPCs within the pores after 14 days of culturing.

The largest transectional surface area of vertical tissue ingrowth through the porosity was measured in the larger 3D-printed version of the implant (Fig. 6D)

Discussion

The main hypothesis that roughening the surface of the elastomer would allow ingrowth of the repair cartilage, resulting in better adherence to the implant, was confirmed. This is already a proven strategy in bone repair, where osteoconductive materials preferably have a porous surface (*Cornell* 1999).

In the attempt to test different pore structures for increased cell infiltration and better mechanical stability of the repair tissue-implant complex, two different concepts of surface manipulation were tested. With both pore-sizes of 319 μm and 775 μm the repair tissue appeared to be tightly connected to the implant and subjectively did not respond differently to manual probing. Admittedly, assessment was qualitative only; in this pilot study no quantitative measurements of maximal shear force resistance were carried out as larger sample numbers would be required to study significance. It lies at hand, however, that larger volumes of ingrowing tissue relate to stronger anchorage of the tissue. The quantity of tissue growing into the pores, was clearly larger in the 3D-L.

The 3D-printed version of the elastomer showed vertical, but no horizontal ingrowth respective to the articular surface, and reached only 100 μm of depth (equal to or even less than 10% of the thickness of the layer of hyaline cartilage in most diarthrodial joints in both horses and humans) in both varieties of the printed elastomer. This might be explained by the fact that in contrast to the native extracellular matrix as found in normal cartilage, the ingrowing repair tissue was surrounded by an inert material with no fluid dynamics. Therefore, the physiologic "pumping mechanism" for nutrient diffusion might have been impaired in deeper layers of the elastomeric 3D structure, preventing deeper ingrowth.

By increasing the porosity of the elastomer in a controlled way, the elastic modulus and yield stress of the elastomer decreased. The elastic modulus ranged from 24.9 $\pm$ 1.2 MPa in the punched version to 3.8 $\pm$ 0.4 MPa in the large pore 3D-printed version. This last value is still well above the elastic modulus for native cartilage (0.45 to 0.80 MPa (*Athanasiou* et al. 1991)). To verify the elastic behavior of the elastomer, a repetitive strain of 20% was applied, representing a high-level strain during human activities (*Sutter* et al. 2015, *Liu* et al. 2010) All three elastomer versions could resist the compressive forces over 20 cycles, without signs of permanent deformation. The recovery percentage of the elastomer was highest for the elastomer with higher porosity whilst the energy dissipation was inversely proportional to the porosity of the implant, being highest for the punched pore elastomer. These results show that the larger total ingrowth volume in the most porous implant did not mean a negative trade-off with respect to its biomechanical characteristics.

In the SE vs. PE experiment the implants on the femoral condyles showed scarce tissue overgrowth when compared to the medial trochlear ridge. The relative distribution of compressive and shear loading across the compartments of the stifle joint varies (*Halley* et al. 2014, *Changoor* et al. 2006, *Moore* and *Burris* 2015). This could explain why tissue overgrowth varied depending on the site of implantation. In the future development of this implant, a site-specific manipulation of porosity might be warranted in order to mimic more closely the local mechanical conditions.

The concept of this treatment would dictate to place the implant completely below the articular surface, in order to

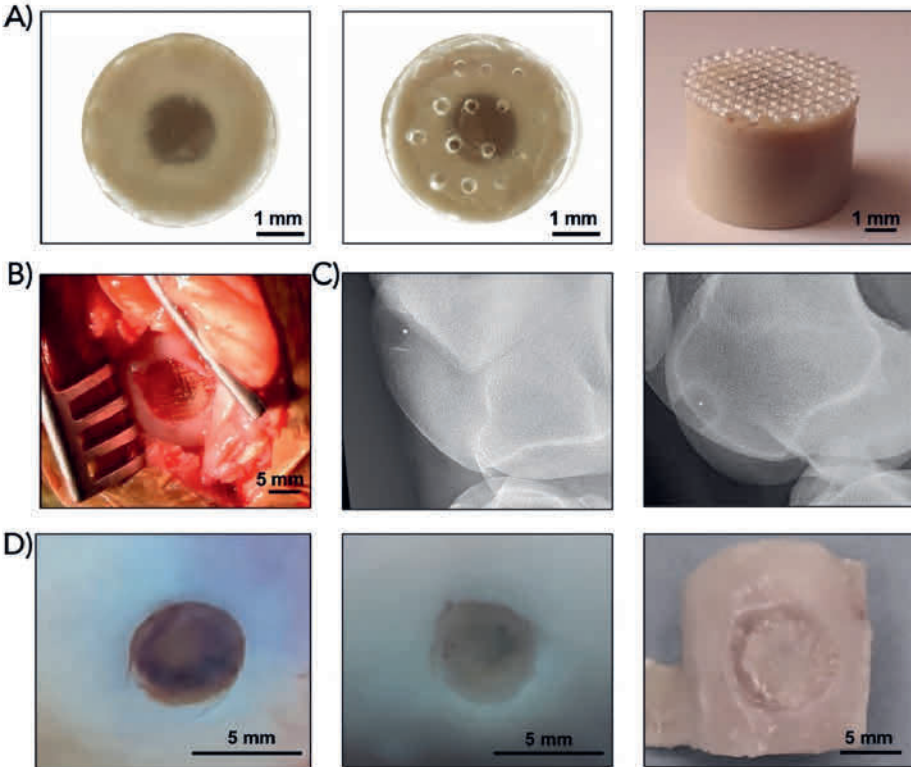

Fig. 4 Three versions of the tested implant. Only the elastomer (chondral component) of the implant varied: smooth elastomer (SE), elastomer with punched pores of 319 μm (PE) and 3D- printed with pores of 690 μm and pores of 775 μm (3D-S and 3D-L; only one version of the 3D printed implants is depicted). B) printed elastomer implanted in the axial aspect of the medial trochlea, 0.5 mm below the articular surface. C) Craniolateral-caudomedial oblique radiographs of two stifles with implant with punched pores and large 3D printed pores. The radiodense area in the middle of the implant represents a metal marker, that was integrated in the implant during fabrication D) Smooth, punched and 3D printed implants on the axial aspect of the medial trochlea, covered with repair tissue, after 5 weeks.

allow tissue overgrowth. This was not possible for two of the 10 mm diameter plugs. Strategies to match the curvature of implants to that of the treated articular surface and to improve the implantation angle are being increasingly sought for (*Heuijerjans* et al. 2018, *Martinez-Carranza* et al. 2014, *Kirker-Head* et al. 2006). The application of a curved radius to the elastomer surface might achieve an improved fitting of the construct below the articular surface in a controlled manner. Hereby a better integration of the entire circumference of the implant could be achieved. As signaled earlier, a major drawback of our approach/design was the lack of objective biomechanical testing of the tissue-covered implant in the post-mortem assessment. Also, a larger number of animals would be necessary in order to provide objectively measured parameters, that can be compared to values of native cartilage or to other repair techniques.

It can be concluded that the surface roughening approach that was investigated in this study indeed succeeded in good adherence of the neo-tissue on the elastomer. This was true for both the punched holes and the printed versions with no visible differences between both approaches. The fact that outcome was similar for both the 6 mm and the 10 mm plugs was encouraging, as the last size is of more clinical relevance than the smaller size. The printing approach resulted in a larger volume of tissue ingrowth and appeared to facilitate manipulation of the biomechanical characteristics of the elastomer. The latter observation is interesting and po-

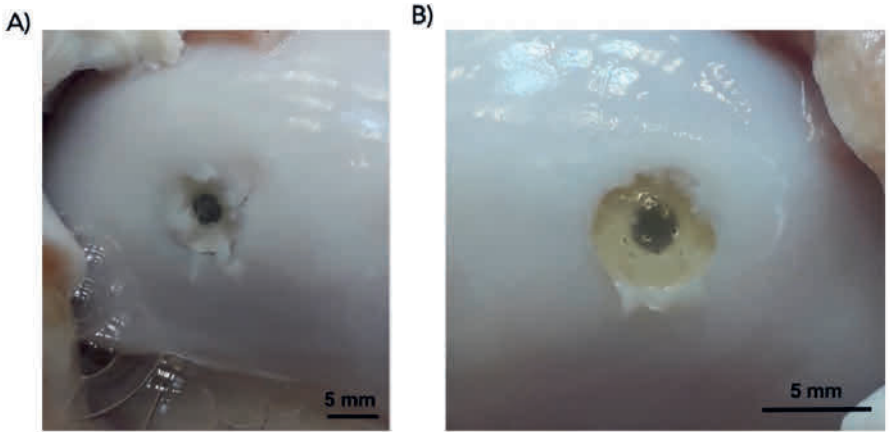

Fig. 5 Implant in situ on the weight bearing surface of the medial femoral condyle, only partially covered with tissue after 5 weeks. A) smooth elastomer B) punched elastomer.

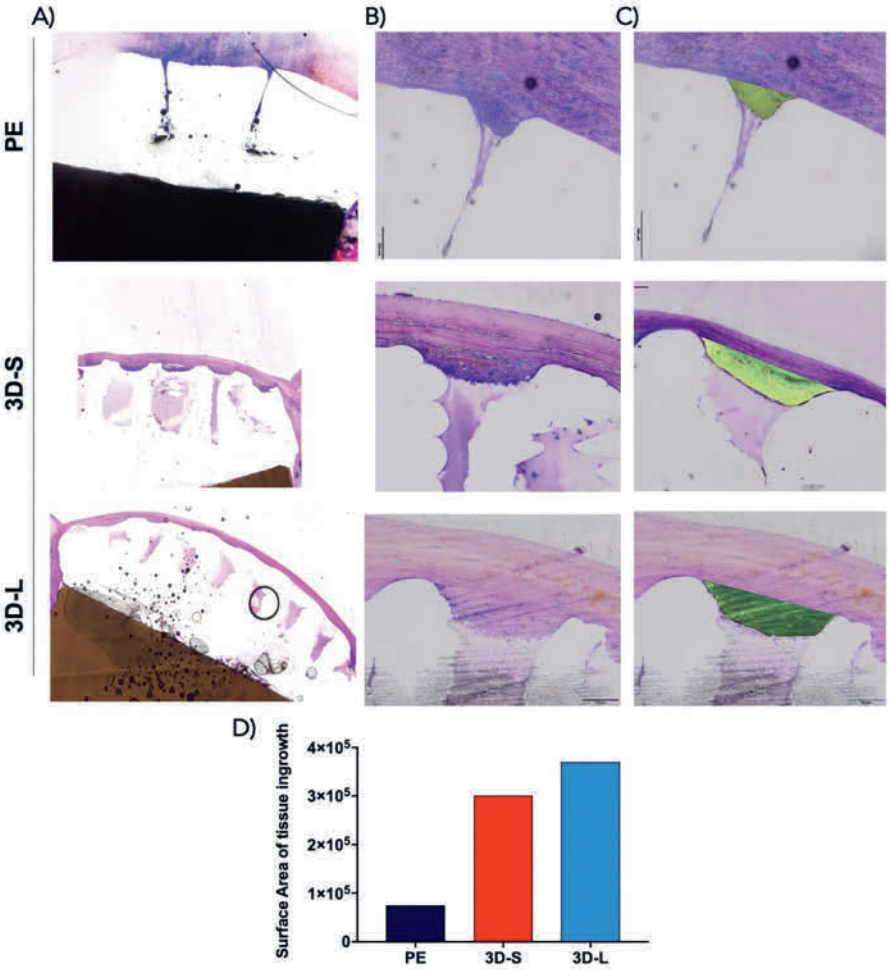

Fig. 6 Representative images of polymethylmethacrylate (PMMA) embedded slides of implants of 6 mm in diameter with microdrilled pores and of polymethylmethacrylate (PMMA) embedded slides of implants with 3D printed elastomer (3D-S and 3D-L), after 5 weeks (1.25x and 2x magnification). The bulging artifact of the elastomer seen in the images is to due the PMMA imbeding process. D) measurement of area of vertical tissue ingrowth in the three implant versions.

tentially enables fine-tuning of the biomechanical properties of the implant depending on the specific requirements for a given location. Considering the short-termed nature of this experiment, the tested implants all showed good mechanical performance *in vitro* and subjectively also *in vivo*. Similarly, from a biological and clinical point of view, no adverse effects were observed. This favorable outcome opens the way for a long-term experimental evaluation of the construct in which the improved adherence and stability of the repair tissue needs to be assessed and quantitatively analyzed in a larger group of animals.

Conflict of interests

Gied Hermsen and Ward van Buul have a financial relationship with JointSphere BV but had no influence on the interpretation of the results.

Declaration of funding

Jointsphere BV covered the material costs of the study.

Ethical approval of animal experimentation

This experiment has been carried out with the approval of the Animal Welfare Body Utrecht (IvD Utrecht,) under the Project number AVD1080020186885 with validity until the 31-01-2024 and work protocol number: 6885-2-1.

References

Athanasiou K. A., Rosenwasser M. P., Buckwalter J. A., Malinin T. I., Mow V. C. (1991) Interspecies comparisons of in situ intrinsic mechanical properties of distal femoral cartilage. J. Orthop. Res. 9, 330–340; DOI 10.1002/jor.1100090304

Becher C., Kalbe C., Thermann H., Paessler H., Laprell H., Kaiser T., Fechner A., Bartsch S., Windhagen H., Ostermeier S. (2011) Minimum 5-year results of focal articular prosthetic resurfacing for the treatment of full-thickness articular cartilage defects in the knee. Arch. Orthop. Trauma Surg. 131, 1135–1143; DOI 10.1007/s00402-011-1323-4

Changoor A., Hurtig M. B., Runciman R. J., Quesnel A. J., Dickey J. P., Lowerison M. (2006) Mapping of donor and recipient site properties for osteochondral graft reconstruction of subchondral cystic lesions in the equine stifle joint. Equine Vet. J. 38, 330–336; DOI 10.2746/042516406777749254

Cornell C. N. (1999) Osteoconductive materials and their role as substitutes for autogenous bone grafts. Orthop. Clin. North Am. 30, 591–598; DOI 10.1016/S0030-5898(05)70112-7

Damen A. H. A., Nickien M., Ito K., van Donkelaar C. C. (2020) The performance of resurfacing implants for focal cartilage defects depends on the degenerative condition of the opposing cartilage. Clin. Biomech. 79, 79:105052; DOI 10.1016/j. clinbiomech.2020.105052

Danielski A., Farrell M. (2018) Use of Synthetic Osteochondral Implants to Treat Bilateral Shoulder Osteochondritis Dissecans in a Dog. Vet. Comp. Orthop. Traumatol. 31, 385–389; DOI 10.1055/s-0038-1651517

Golafshan N., Willemsen K., Kadumudi F. B., Vorndran E., Dolatshahi-Pirouz A., Weinans H., van der Wal B. C. H., Malda J., Castilho M. (2021) 3D-Printed Regenerative Magnesium Phosphate Implant Ensures Stability and Restoration of Hip Dysplasia. Adv. Healthcare Mat. 2101051; DOI 10.1002/ADHM.202101051

Halley S. E., Bey M. J., Haladik J. A., Lavagnino M., Arnoczky S. P. (2014) Three dimensional, radiosteriometric analysis (RSA) of equine stifle kinematics and articular surface contact: A cadaveric study. Equine Vet. J. 46; 364–369; DOI 10.1111/evj.12127

Heuijerjans A., Wilson W., Ito K., van Donkelaar C. C. (2018) Osteochondral resurfacing implantation angle is more important than implant material stiffness. J. Orthop. Res. 36, 2911; DOI 10.1002/JOR.24101

Husby K. A, Reed S. K., Wilson D. A., Kuroki K., Middleton J. R., Hoepp N. C., Charles E. M., Cook J. L. (2016) Evaluation of a Permanent Synthetic Osteochondral Implant in the Equine Medial Femoral Condyle. Vet. Surg. 45, 364–373; DOI 10.1111/vsu.12453

Hunziker E. B. (1999) Articular cartilage repair: Are the intrinsic biological constraints undermining this process insuperable? Osteoarthr. Cartil. 7,15–28; DOI 10.1053/joca.1998.0159

Kirker-Head C. A., van Sickle D. C., Ek S. W., McCool J. C. (2006) Safety of, and biological and functional response to, a novel metallic implant for the management of focal full-thickness cartilage defects: Preliminary assessment in an animal model out to 1 year. J. Orthop. Res. 24, 1095–1108; DOI 10.1002/JOR.20120

Korthagen N. M, Brommer H., Hermsen G., Plomp S. G. M., Melsom G., Coeleveld K., Mastbergen S. C., Weinans H., van Buul W., van Weeren P. R. (2019) A short-term evaluation of a thermoplastic polyurethane implant for osteochondral defect repair in an equine model. Vet. J. 251, 105340; DOI 10.1016/j.tvjl.2019.105340

Liu F., Kozanek M., Hosseini A., Van de Velde S. K., Gill T. J, Rubash H. E., Li G. (2010) In vivo tibiofemoral cartilage deformation during the stance phase of gait. J. Biomechanics 43, 658–665; DOI 10.1016/J.JBIOMECH.2009.10.028

Mankin H. J. (1982) The response of articular cartilage to mechanical injury. J. Bone Joint Surg. Am. 64, 460–466; DOI

Martinez-Carranza N., Hultenby K., Lagerstedt A. S., Schupbach P., Berg H. E. (2019) Cartilage Health in Knees Treated with Metal Resurfacing Implants or Untreated Focal Cartilage Lesions: A Preclinical Study in Sheep. Cartilage 10, 120–128; DOI 10.1177/1947603517720260

Martinez-Carranza N., Ryd L., Hultenby K., Hedlund H., Nurmi-Sandh H., Lagerstedt A. S., Schupbach P., Berg H. E. (2016) Treatment of full thickness focal cartilage lesions with a metallic resurfacing implant in a sheep animal model, 1 year evaluation. Osteoarthr. Cartil. 24, 484–493; DOI 10.1016/j.joca.2015.09.009

Martinez-Carranza N., Berg H. E., Lagerstedt A. S., Nurmi-Sandh H., Schupbach P., Ryd L. (2014) Fixation of a double-coated titanium-hydroxyapatite focal knee resurfacing implant: A 12-month study in sheep. Osteoarthr. Cartil. 22, 836–844; DOI 10.1016/j.joca.2014.03.019

Moore A. C., Burris D. L. (2015) Tribological and material properties for cartilage of and throughout the bovine stifle: Support for the altered joint kinematics hypothesis of osteoarthritis. Osteoarthr. Cartil. 23; 161–169; DOI 10.1016/j.joca.2014.09.021

Nathwani D., McNicholas M., Hart A., Miles J., Bobić V. (2017) Partial Resurfacing of the Knee with the BioPoly Implant. J.Bone Joint Surg. Open Access 2, e0011; DOI 10.2106/jbjs.oa.16.00011

Sutter E., Widmyer M., Utturkar G., Spritzer C. E., Garrett W. E., DeFrate L. E. (2015) In vivo measurement of localized tibiofemoral cartilage strains in response to dynamic activity. Am. J. Sports Med. 43, 370–376; DOI 10.1177/0363546514559821

Supplementary material and methods

1. Filament fusion test

For the filament fusion test, the elastomer was printed in meandering patterns composed of parallel strands at increasing spacings, from 0.5 mm to 1 mm (Fig. S2) After taking pic-

tures, the fused segment length (fs) at each filament distance (fd) were measured using ImageJ and normalized by dividing fs by the average of filament thickness (ft) to avoid the effect of filament thickness variation. At least 3 measurements used for the quantification and the images were recorded by a stereomicroscope (Olympus SZ61, magnification 4.2×, resolution 2040 × 1536 pixels) immediately after printing.

2. Mechanical characterization of implants

The elastic modulus (defined as the slope of the linear region from 0.1 to 0.2 mm/mm), the stress (defined as the stress at 0.2 mm/mm strain), and the strain energy (defined as the absorbed energy by the scaffolds up to yield stress) were determined.

Further, the elastic behavior of the implants, was assessed under dynamic compression. From the dynamic tests, the dissipated energy was assessed by the loss of energy after the unloading. In addition, the recovery was calculated by dividing the loaded energy of the 20th cycle by the loaded energy of the 1st cycle.

Culturing protocol

The implants were cultured in DMEM (high glucose, GlutaMAX-TM, pyruvate) (Gibco, USA), 10% FBS (Biowest, France), 10µl/ml pen/strep (Gibco, USA), 5µl/ml ASAP (Sigma, USA), and 1µl/ml (-FGF (R&D Systems, USA). Medium was changed every 3 days.

3. Cell imaging technique

In order to image the cells within the scaffolds, the cells were fixed in formalin, washed with 0.2%Triton in PBS for 10 min and stained with DAPI solution. Subsequently the cells were imaged with a confocal microscope (Leica SP8X Laser Scanning, Germany) with 358 nm and 461 excitation filters, and 3 samples were analysed per group per timepoint.

4. Inclusion criteria and surgical pre- and post-operative protocol

The ponies were admitted to the clinic 2 weeks prior to surgery to acclimate to the environment. They were fed on hay (2% body weight) and had free water access. Clinical lameness examination was performed by the author assist-

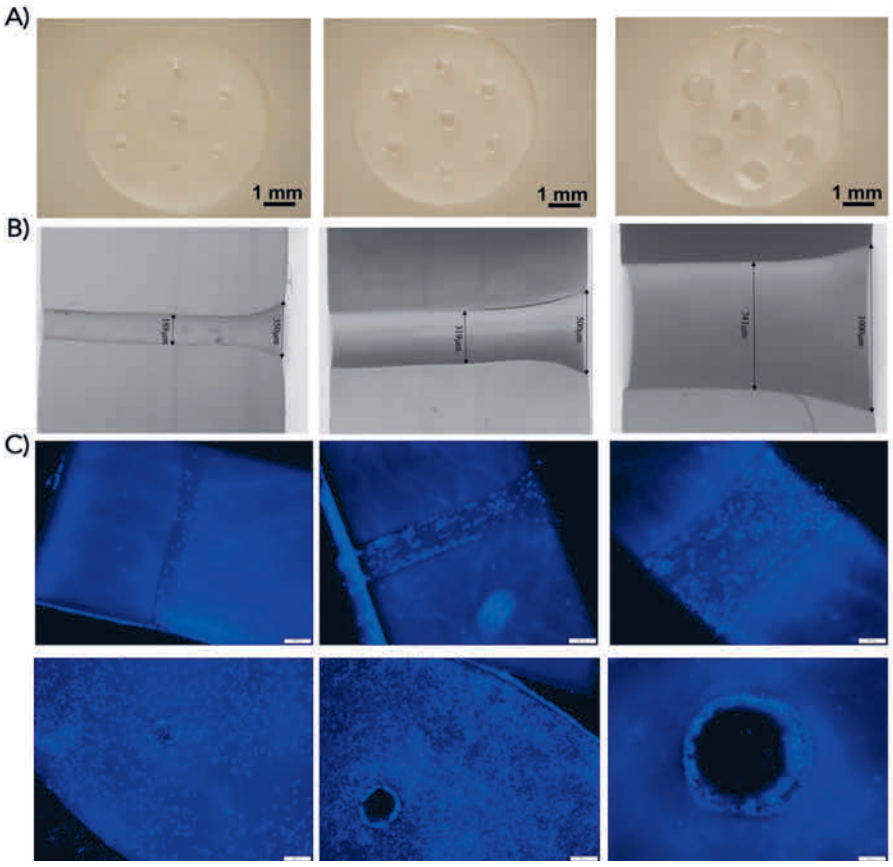

Fig. S1 A) Images of the punched elastomer with different pore sizes. B) The cross-section images of the punched elastomer to show the inner diameter. C) DAPI staining of in pores infiltrated ACPCs after 14 days of culturing for the punched elastomers with different pore sizes.

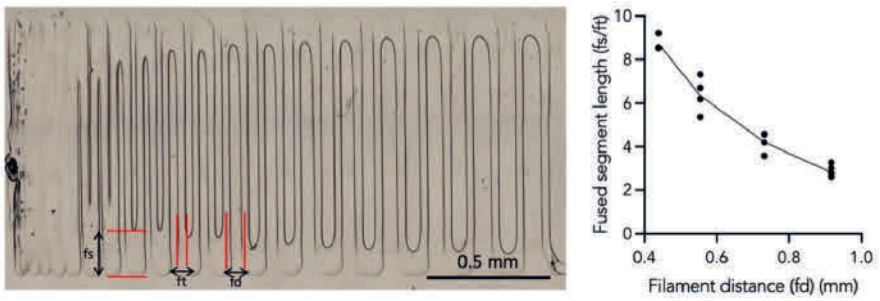

Fig. S2 Filament fusion test for printability evaluation of PCUU. fs: filament segment length; ft: filament thickness; fd: filament distance.

ed by a quantitative gait analysis device (EquiMoves). All animals were clinically sound and lame-free. Radiographic images on four projections of the stifle (antero-posterior, latero-medial, dorsolateral-caudomedial and dorsomedial – caudolateral) were obtained pre-operatively. Only ponies with normal radiographic appearance were included in the study. On the day of surgery, ampicillin (10–15 mg/kg IV), gentamicin (6.6 mg/kg IV) and meloxicam (0.6 mg/kg) were administered through a previously placed jugular vein catheter. The ponies were then sedated with detomidine (10 mcg/kg IV) and morphine (0.1 mg/kg IV). General anesthesia was induced with midazolam (0.06 mg/kg) and ketamine (2.2 mg/kg) and maintained with isoflurane in oxygen through endotracheal tubing and a continuous rate infusion (CRI) of detomidine (10 mcg/kg/h) and ketamine (0.5 mg/kg/h).

Postoperatively a single dose of procaine penicillin (20 mg/kg im) was administered and meloxicam (0.6 mg/kg) and morphine (0.1 mg/kg) where administered orally twice a day for 3 days. Ponies were daily assessed for clinical parameters and lameness and were box-rested for 5 weeks. A lameness examination was performed by the author assisted by a quantitative gait analysis device (EquiMoves®)

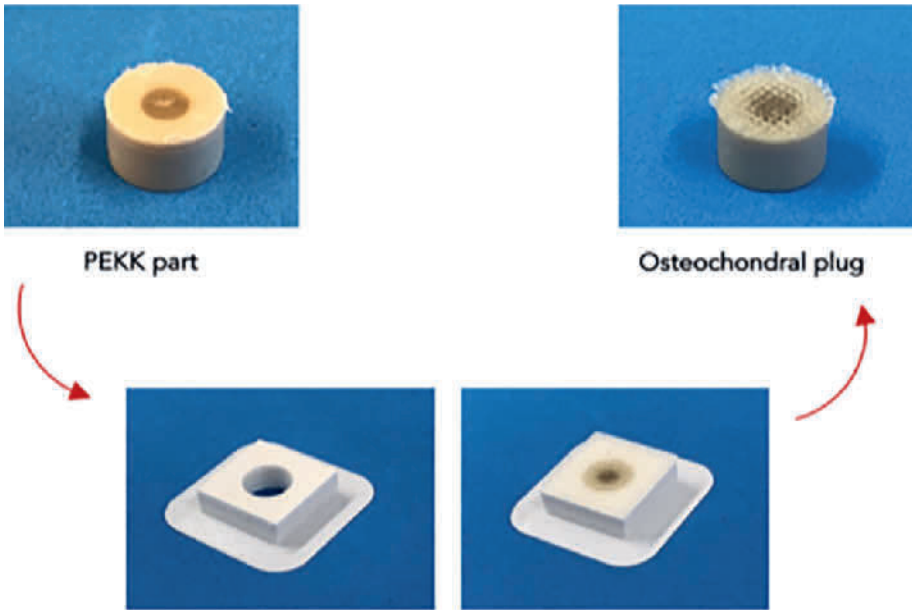

Fig. S3 3D fabrication procedure of the 3D- printed implants.

Pferdeheilkunde – Equine Medicine 39 (2023) 6 (November/December) 515–522 DOI 10.21836/PEM20230602

Occurrence of elevated amylase and lipase enzymes in horses with gastrointestinal disease

Helena Bartel[1], Astrid B. M. Rijkenhuizen[2], Cora-C. Sommerey[3], Graham Stock[3] and Katja Shell[1]

[1] Pferdeklinik Leichlingen GmbH, Leichlingen, Germany
[2] European Equine Surgeon Consultant, Wijk bij Duurstede, The Netherlands
[3] IDEXX GmbH, Kornwestheim, Germany

Summary: Pancreatic disease in horses is rare and diagnosis is difficult due to lack of available diagnostic tests. Acute pancreatitis is associated with acute colic signs and gastrointestinal reflux; chronic pancreatitis with weight loss, anorexia, lethargy, and mild recurrent colic symptoms. Therefore, horses presented with such unspecific symptoms are often treated routinely and a concurrent pancreatic disorder may be missed. A prospective study was initiated to investigate the occurrence of pancreatic disease in horses with corresponding clinical signs. During the study period from 2018–2019, sixty-seven horses (39 geldings, 26 mares, 2 stallions) aged 1–26 years with Warmbloods being the predominant breed were included. In 48 horses, the pancreatic enzymes α-amylase (AMY) and DGGR-lipase (LIP) were measured in serum (S) and peritoneal fluid (PF). In addition, cytologic examination from PF, complete blood count (CBC) and serum biochemistry (SBC) were performed. In 19 horses, including 14 control horses without clinical signs, pancreatic enzymes were measured from serum samples only. In one horse with colic symptoms, LIP was elevated in S; in another horse with duodenitis-proximal jejunitis and septic peritonitis, LIP was elevated in PF. In both horses, a pancreatic component was considered to play a role. A third horse had measured enzymes within normal ranges, but postmortem examination revealed chronic pancreatitis. These results suggest that pancreatic disease has a low prevalence in horses, but should be considered as an additional differential diagnosis in patients with indistinct abdominal symptoms.

Keywords: pancreatitis, horse, amylase, lipase, colic symptoms

Citation: Bartel H., Rijkenhuizen A. B. M., Sommerey C.-C., Stock G., Shell K. (2023) Occurrence of elevated amylase and lipase enzymes in horses with gastrointestinal disease. Pferdeheilkunde 39, 515–522; DOI 10.21836/PEM20230602

Correspondence: Helena Bartel, Pferdepraxis Dr. Martin Thunig, Dr.-C.-Otto-Str. 117, 44879 Bochum, Germany; helena.ariane.bartel@gmail.com

Submitted: Juli 18, 2023 | **Accepted:** September 24, 2023

Introduction

Pancreatic disease has been described for decades as a rare disorder in equids and is diagnosed mostly at necropsy due to lack of available and reliable antemortem diagnostic tests (*Higginson* 1937, *Talbot* et al. 2011, *Yamout* et al. 2012, *Edery* et al. 2015, *Newman* 2015). Both primary and secondary pancreatitis can occur. Primary pancreatitis is defined as pancreatic lesions as the main or only pathological finding, whereas secondary pancreatitis occurs as a result of any other underlying disorder (*Yamout* et al. *2012*).

Postmortem findings include acute, chronic and chronic active pancreatitis (*Breider* et al. 1985, *Taintor* et al. 2006, *Bakos* et al. 2008, *Talbot* et al. 2011, *Ollivett* et al. 2012, *Yamout* et al. 2012, *Newman* 2015) and neoplasia (*Ross* et al. 1983, *Church* et al. 1987, *Carrick* et al. 1992, *Rendle* et al. 2006, *Barsnick* et al. 2008, *Spanton* et al. 2009, *Brot* et al. 2014, *Herbach* et al. 2014).

Diagnosing pancreatitis remains challenging. Whereas acute pancreatitis in adult horses is characterized by severe abdominal pain, ileus with duodenogastric reflux and hypovolemia (*Bakos* et al. 2008, *Schmidt* et al. 2010, *Yamout* et al. 2012, *Newman* 2015, *Lack* et al. 2020), chronic pancreatitis presents with weight loss, lethargy, mild recurrent colic and inappetence (*Breider* et al. 1985, *Yamout* et al. 2012, *Leipig* et al. 2015). Coma and cerebral dysfunction as predominant clinical findings have been reported in two cases of severe acute pancreatitis in foals (*Taintor* et al. 2006, *Ollivett* et al. 2012). Currently there is no standardized test to diagnose pancreatitis in horses. Elevated serum enzyme activities of amylase (AMY) and lipase (LIP), secreted by the acinar cells of the pancreas, are considered useful to diagnose acute pancreatic disease in horses, although they are of limited diagnostic accuracy.

For diagnosing acute pancreatitis in humans, measurement of LIP is preferred because it is tissue-specific and has a sensitivity between 64% and 100%, whereas sensitivity of AMY for diagnosis of acute pancreatitis is between 45% and 87% (*Ismail* and *Bhayana* 2017). The specificities for both enzymes range between 92% and 99%. LIP has a larger time slot than AMY, as it rises 3–6 hours after onset of clinical signs and remains elevated for up to two weeks, whereas AMY peaks rapidly after the onset of clinical signs, has a short half-life of 10–12 hours and returns to normal within three to five days (*Ismail* and *Bhayana* 2017).

In recent research, the 1′2-o-dilauryl-rac-glycero-3-glutarate- (6′-methylresorufin) ester (DGGR) lipase assay has been determined to be a pancreas-specific parameter in horses (*Johnson* et al. 2019). Determination of DGGR-LIP (LIP) and AMY in horses is expected to be of diagnostic value for pancreatic disease, although AMY has limitations as a single assay. AMY activity in the pancreas is low (*Lorenzo-Figueras* et al. 2007, *Johnson* et al. 2019) and activity of AMY is a one-half LIP half-life period in plasma (*Johnson* et al. 2019). Besides, hyperamylasemia can also occur in intestinal and renal disorders (*Clink* et al. 1982), which are more common than pancreatic disease. This preliminary research aimed to investigate the occurrence of elevated pancreatic enzymes (AMY and LIP) in horses with gastrointestinal disorders in serum (S) and peritoneal fluid (PF). The objective was to determine if measurement of pancreatic enzymes can be helpful as a screening tool to identify horses with pancreatic disease ante mortem and to document clinical cases. The study hypothesis was that pancreatic disease occurs in horses with clinical signs of gastrointestinal disease.

Material and methods

The study was performed from 2018 to 2019 and included 67 horses (39 geldings, 26 mares, 2 stallions) aged 1–26 years (median age 13 years) with Warmbloods being the predominant breed (50.7%), divided into two groups. Group A included 53 horses, which were presented for diagnostic workup of gastrointestinal and hepatic disease with one or more of the following symptoms: acute colic signs with and without duodenogastric reflux, peritonitis, weight loss, anorexia, lethargy, mild recurrent colic symptoms and elevated liver enzymes. The pancreatic enzymes AMY and LIP were measured in S and PF samples taken at admission. Unfortunately, in five horses no peritoneal fluid could be obtained. Complete blood count (CBC) and serum biochemistry (SBC) were performed as point-of-care examinations (IDEXX ProCyte, IDEXX Catalyst One). Cytology from PF was performed at the IDEXX reference laboratory. Group B included 14 clinically healthy horses as negative control group, presenting for orthopedic complaints without signs of gastrointestinal disease (5 geldings, 8 mares, 1 stallion, median age 12.5 years). In these horses, routine blood work was performed, and available samples served for measurement of AMY and LIP. For this study, institutional animal care and use committee approval was not required as residual material from routine diagnostic work-up was used. Owner consent was obtained for use of remaining samples for research purposes.

Blood samples were centrifuged and serum was refrigerated at 4 °C. Peritoneal fluid samples were smeared immediately after sampling and the remainder equally refrigerated at 4 °C until handling in the laboratory. All samples were sent overnight and analyzed at the IDEXX reference laboratory the following day and results were available 1–2 days after sending.

Enzymes were measured by photometry, for lipase an enzymatic colorimetric assay with 6-methyl-resorufin ester as substrate (Roche; Beckman Coulter AU680 clinical chemistry analyzer) was performed. Alpha amylase was measured by a kinetic colorimetric assay with ethylidene-G7PNP as substrate (Beckman Coulter; Beckman Coulter AU680 clinical chemistry analyzer). Reference values for LIP (laboratory specific internal validation) were serum activity < 250 international units per litre (IU/L) and 0–400 IU/L for AMY (Kraft Dürr, Klinische Labordiagnostik, 5. Auflage, Schattauer Verlag, 1999). For PF, laboratory-specific reference ranges were not available. Cytologic examinations of PF were performed of direct smears and after cytospin, May-Grünwald-Giemsa staining was conducted (IDEXX GmbH).

Results

In group A, mean S AMY was 14.5 IU/L, S LIP 27 IU/L, PF AMY 12.9 IU/L, and PF LIP 27.44 IU/L. Based on the enzyme activities, two horses were suspected to have a pancreatic disease.

Details of these two cases are described in detail, as well as a third horse, which had normal enzyme activities but post-mortem diagnosis of chronic pancreatitis. In group B, serum enzymes were within the reference ranges in all cases, mean S AMY was 10.8 IU/L, mean S LIP was 13 IU/L.

Clinical cases

Case 1

Case 1 was a 20-year-old Appaloosa mare, presenting with colic symptoms of one day duration. Treatment by the referring veterinarian consisted of N-butylscopolamine (0.2 mg/kg per bodyweight [bwt] intravenously [IV], metamizol-natrium 25 mg/kg bwt IV, Buscopan comp.®)[a] and butorphanol (Torbugesic®Vet, 0.01 mg/kg bwt IV)[b]. Two months before presentation the horse underwent celiotomy due to large colon displacement in another hospital.

On arrival, the horse showed mild signs of abdominal discomfort, vital parameters were within normal ranges. Nasogastric intubation revealed no net reflux, feed was obtained during flushing. Transrectal palpation and transabdominal ultrasound examination (5–2 MHz-probe, Sonosite®)[c] were unremarkable.

CBC showed a mild hypochromic anemia (packed cell volume [PCV] 0.23 L/L, reference range [rr] 0.32–0.40 L/L). Red blood cells (RBC) were decreased (5.07 T/L, rr 6.4–10.4 T/L), haemoglobin was 8.8 mmol/L (rr 10.7–16.5 mmol/L).

Abdominocentesis revealed clear peritoneal fluid with a normal total nucleated cell count ([TNCC] 3.4×10^9/L, rr $< 5.0 \times 10^9$/L), lactate (0.89 mmol/L, rr < 1.78 mmol/L), and total protein ([TP] 12 g/L, rr < 25 g/L). Cytology of the abdominal fluid was unremarkable.

Another period of mild colic three hours later resolved after administration of N-butylscopolamine (0.2 mg/kg bwt IV), and metamizol-natrium (25 mg/kg bwt IV, Buscopan comp®)[a].

Gastroscopy (gastroscope, 320 cm, STORZ®)[d] was performed the following day. The stomach was still filled with gastric content despite fasting for 14 hours. After treatment with metoclopramide (0.25 mg/kg IM every 6 hours, Metomotyl®)[e], the stomach was completely empty the next day and the gastric

mucosa was unremarkable in all aspects. The horse was re-fed and did not show clinical signs of discomfort again. Diagnosis was spasmodic colic with secondary gastric dilation and repeated CBC due to mild anemia was recommended. The owner reported that the mare was doing well a few days after discharge.

Laboratory results of AMY, LIP and cytology arrived after discharge of the horse. Serum AMY was within the reference range measured 189 IU/L, S LIP was 489 IU/L (rr < 250 IU/L). In PF, AMY was 39 IU/L and LIP measured 105 IU/L.

The elevated LIP activity in S was suggestive of concurrent pancreatitis. In PF, LIP activity was also high in comparison to reference ranges of S, as there are no laboratory specific reference ranges for PF.

Cytology of the abdominal fluid was unremarkable.

Case 2

A 9-year-old Haflinger gelding presented due to acute colic symptoms for a few hours and suspected small intestinal obstruction. The horse was referred after administration of flunixine-meglumine (1.1 mg/kg bwt IV, Flunidol®)[f] and obtaining 10 L of duodenal reflux into the stomach by nasogastric intubation.

On arrival, the horse was reduced in behaviour, tachycardic (heart rate 56 beats per minute [bpm]) and showed mild signs of colic. Capillary refill time was prolonged and nasogastric intubation revealed 5 L of duodenogastric reflux. Routine blood work showed mild haemoconcentration (PCV 0.38 L/L, rr 0.32–0.40 L/L) with hyperproteinemia (87 g/L, rr 56–79 g/L) and hyperalbuminemia (34 g/L, rr 19–32 g/L), neutrophilic leucocytosis with left shift (WBC 12.97 G/L, rr 4.9–11.1 G/L), elevation of Alkaline Phosphatase ([ALKP] 829 U/L, rr 10–326 U/L), elevated ɣ-Glutamyltransferase ([GGT] 181 U/L, rr 0–87 U/L), increased globulin (53 g/L, rr 24–47 g/L) and hyperglycemia (9.05 mmol/L, rr 3.55–8.32 mmol/L). Mild colon impaction of the flexura pelvina was palpated transrectally, transabdominal ultrasound examination showed increased free abdominal fluid and a few distended small intestinal loops. Peritoneal fluid obtained by abdominocentesis was turbid with an elevated TNCC 21.77×10^9/L (rr < 5.0×10^9/L) and elevated lactate of 5.1 mmol/L (rr < 1.78 mmol/L).

Due to severe signs of colic, diagnostic laparotomy via ventral midline incision was performed immediately and enteritis was diagnosed. The amount of peritoneal fluid was increased and turbid. The flexura pelvina of the colon ascendens was impacted and slightly displaced to the right side, the caecum was displaced caudally. The stomach was distended with gas, the jejunum was gas-distended and showed marked hypomotility, the ileum wall was thickened. An enteritis was suspected on base of the findings during surgery. Full-thickness biopsies from jejunum and ileum showed marked oedema of the intestinal wall at histopathologic examination without signs of inflammation.

Serum AMY (< 10 IU/L) and LIP (80 IU/L) were within normal ranges. In PF, both enzymes were elevated compared to serum values, AMY was 342 IU/L and LIP measured 706 IU/L. Cytology revealed an inflammatory peritoneal effusion of increased cellularity with a high amount of partially degenerated neutrophil granulocytes. Bacterial culture growth of *E. coli ssp*. with haemolysis was present. Diagnosis of septic peritonitis was made. Based on the high activities of PF AMY and LIP concurrent pancreatitis was suspected. Cytology results and enzyme activities were available one day after surgery.

Postoperative treatment consisted of lidocaine (Lidocainhydrochloride 2%®)[g] as constant-rate infusion ([CRI], 0.05 mg/kg/hour after initial bolus of 1.3 mg/kg/hour over 15 minutes), procain penicillin G (Procain Penicillin G®, 22.000 IU/kg IM once daily)[h], gentamicin (Gentacin®, 6.6 mg/kg IV once daily)[i], metronidazole (Metrobactin®,15 mg/kg orally every 8 hours)[i], flunixin-meglumine (Flunidol®, 0.5 mg/kg IV every 12 hours)[f] for 5 days and fluid therapy (Braun NaCl 0.9%®, saline 0.9% in combination with balanced electrolyte solution, Ursolyt 153S® 90 ml/kg/24 hours)[k,l]. Nasogastric intubation was performed every 6 hours during the first day, and duodenogastric reflux was not observed after surgery. Vital parameters were within normal ranges, borborygmi, defaecation and behaviour were normal. The horse was offered water and a handful hay and mash 24 hours postoperatively, but appetite was reduced. Gastroscopy was performed 4 days postoperatively. The stomach was filled with gastric content despite restricted feeding and fasting for 14 hours. Due to delayed emptying metoclopramide was administered (Metomotyl®, 0.25 mg/kg IM every 6 hours)[e] before gastroscopy was repeated the next day. The stomach was empty then and mild, equine glandular gastric disease (EGGD) was observed as multifocal, hyperemic lesions of the pylorus as well as mild inflammation of the duodenal mucosa. Duodenal biopsies revealed a neutrophilic inflammation with evidence of mucosal barrier disruption.

Medical therapy with betanechol (Myocholine Glenwood®, 0.05 mg/kg orally every 8 hours)[m] and sucralfate (Sucralfat®, 12 mg/kg every 12 hours)[n] was initiated. The horse started eating and showed normal appetite. Five days postoperatively, ventral oedema and mild purulent exudation at the incision site were apparent. Daily wound cleaning was performed.

Behaviour was normal and the remainder of the postoperative period was uneventful until discharge eight days postoperatively. The horse was fed with maintenance requirements of hay and mash at discharge, the owner was advised to start handwalking 5 minutes daily.

At re-examination four weeks later, wound healing was advanced. The owner reported of an uneventful recovery, without any signs of gastrointestinal disease. Gastroscopy still revealed mild EGGD of the pyloric region in addition to equine squamous gastric disease (ESGD), grade I/IV, gastric emptying was normal. Abdominocentesis was performed for monitoring and revealed turbid fluid with an elevated TNCC of 17.44×10^9/L (rr < 5.0×10^9/L) and elevated total protein of 40 g/L (rr < 20 g/L). Based on cytological findings, a modified transudate with a mixed cell population and small amounts of non-degenerated neutrophils was diagnosed without indication of septic inflammation. Serum AMY was < 10 IU/L, serum LIP was 13 IU/L, AMY in PF was 0 IU/L and LIP in PF